FULL PAPER

Pyrolysed 3D-Carbon Scaffolds Induce Spontaneous Differentiation of Human Neural Stem Cells and Facilitate Real-Time Dopamine Detection

*Letizia Amato, Arto Heiskanen, Claudia Caviglia, Fozia Shah, Kinga Zór, Maciej Skolimowski, Marc Madou, Lauge Gammelgaard, Rasmus Hansen, Emma G. Seiz, Milagros Ramos, Tania Ramos Moreno, Alberto Martínez-Serrano, Stephan S. Keller, and Jenny Emnéus**

Structurally patterned pyrolysed three-dimensional carbon scaffolds (p3D-carbon) are fabricated and applied for differentiation of human neural stem cells (hNSCs) developed for cell replacement therapy and sensing of released dopamine. In the absence of differentiation factors (DF) the pyrolysed carbon material induces spontaneous hNSC differentiation into mature dopamine-producing neurons and the 3D-topography promotes neurite elongation. In the presence and absence of DF, ≈73–82% of the hNSCs obtain dopaminergic properties on pyrolysed carbon, a to-date unseen efficiency in both two-dimensional (2D) and 3D environment. Due to conductive properties and 3D environment, the p3D-carbon serves as a neurotransmitter trap, enabling electrochemical detection of a significantly larger dopamine fraction released by the hNSC derived neurons than on conventional 2D electrodes. This is the first study of its kind, presenting new conductive 3D scaffolds that provide highly efficient hNSC differentiation to dopaminergic phenotype combined with real-time in situ confirmation of the fate of the hNSC-derived neurons.

1. Introduction

Dopamine, a member of the catecholamine family, acts as a neurotransmitter in the central nervous system (CNS), modulating vital CNS functions, such as voluntary movement. In Parkinson's disease (PD) patients, dopamine releasing (dopaminergic) neurons in the CNS are dysfunctional or dying, causing a lack of dopamine in the target territories, which leads to impaired motor functions.[1] One of the suggested therapeutic approaches to restore dopamine production in PD patients is transplantation of cells that acquire dopaminergic phenotype (cell replacement therapy, CRT) in the brain of these patients.[1,2] Intensive research is ongoing to evaluate the potentials of different cellular precursors, such as embryonic (ESC), induced pluripotent (iPSC), and fetal neural stem cells (NSC), each type having both advantages and disadvantages. NSCs from fetal mesencephalon are considered to provide a sustainable source of transplantable cells becoming dopaminergic neurons[2] associated with lower tumorigenicity than, e.g., ESCs and iPSCs.[1] An important goal is that a large fraction of the NSCs acquire dopaminergic phenotype while minimizing the formation of other type of neurons and glial cells. To standardize and enhance differentiation of NSCs to dopaminergic neurons in

Dr. L. Amato, Dr. A. Heiskanen, C. Caviglia, F. Shah, Dr. K. Zór, Dr. M. Skolimowski,[+] R. Hansen, Dr. S. S. Keller, Prof. J. Emnéus
Technical University of Denmark
Department of Micro- and Nanotechnology (DTU Nanotech)
Produktionstorvet 423
DK-2800, Kgs. Lyngby, Denmark
E-mail: jenny.emneus@nanotech.dtu.dk

Prof. M. Madou
Department of Mechanical & Aerospace Engineering
University of California
Irvine, CA 92697, USA

Dr. L. Gammelgaard
Capres A/S, Diplomvej 373
DK-2800, Kgs. Lyngby, Denmark

Dr. E. G. Seiz, Dr. M. Ramos, Dr. T. Ramos Moreno,[++] Prof. A. Martínez-Serrano
Departmento de Biología Molecular and Centro de Biología Molecular "Severo Ochoa" (CBMSO)
Universidad Autónoma de Madrid – C.S.I.C., Cantoblanco
28049 Madrid, Spain

[+]Present address: University of Groningen, Department of Pharmacy, Antonius Deusinglaan 1, Postbus 196, 9700 AD Groningen, The Netherlands
[++]Present address: Lund University, Wallenberg Neurocentrum, BMC, Sölvegatan 17, SE-22100 Lund, Sweden

DOI: 10.1002/adfm.201400812

in vitro studies, cell signaling and gene expression are controlled using, for example, neurotrophic factors[3,4] (hereafter referred to as differentiation factors, DF), as well as genetic modifications.[4,5] Expansion of the cell populations, while suppressing differentiation, is achieved using different growth factors (GF).

Typically, NSC studies rely on two-dimensional (2D) cultures on commercial tissue culture polystyrene (TCPS). Properties of the differentiated NSCs are determined by indirect means using, for instance, immunocytochemistry (ICC), quantitative real-time PCR (qPCR) and Ca^{2+} imaging, which only show the appearance of intermediate biomarkers.[4,6,7] In the case of differentiation to dopaminergic neurons, the released dopamine is typically quantified by high performance liquid chromatography (HPLC) analysis in collected culture medium samples.[4,6] To date, differentiation of human NSCs (hNSC) in the presence of DF has yielded maximally about 17–18% of dopaminergic neurons in entire populations of hNSCs, whereas without the application of DF only about 2% of the cells are showing dopaminergic properties.[4,5] Confirmation of true dopaminergic phenotype of hNSC-derived neurons requires, however, real-time detection of the actually released dopamine upon depolarization (exocytosis), which is only possible by electrochemical detection. Real-time detection of dopamine exocytosis has been demonstrated on single cells and cell populations belonging to different model cell lines, for example, pheochromocytoma (PC12) cells, releasing catecholamines, the most abundant of which is dopamine.[8] Exocytosis measurements have been conducted using either carbon fiber microelectrodes (CFME)[9,10] or planar (2D) microelectrode chips.[11–14] However, to our best knowledge, no studies have reported electrochemical real-time detection of dopamine released by depolarized hNSCs.

Novel materials, structures and tools are therefore essential for the field of stem cell research and CRT to boost and guide differentiation to specific neuronal lineages, as well as to facilitate real-time evaluation of the fate of NSC-derived neurons. A range of different materials[15,16] is currently being explored for building three-dimensional (3D) scaffolds for tissue engineering and biomedical research. The 3D environment is envisaged to provide a better mimic of the natural in vivo environment, leading to more physiologically realistic and reliable biomedical research tools than currently used standard 2D formats.[17,18] Polymeric microtowers[18] and superhydrophobic silicon micropillars[19] have proven to provide an optimal 3D microenvironment for neuron-astrocyte co-cultures, promoting formation of neuronal networks. 3D peptide nanowire scaffolds have boosted rodent stem cell differentiation into dopaminergic phenotype.[6] In a longer perspective, 3D scaffolds will be the key to building artificial tissues, organs, and implants,[16] which can provide new possibilities for CNS regeneration and specifically CRT.

Conductive 3D scaffolds have emerged, providing both structural support and means to electrically stimulate and/or monitor a cell population.[20–23] They are of particular interest in neuroscience due to the inherent neuronal electroactivity. Although carbon nanomaterials, for example, carbon nanotubes (CNTs) and graphene, are highly conductive, their advantages have been primarily demonstrated as 2D scaffolds/substrates for neuronal and neural stem cell cultures. CNTs have been shown to increase the activity of neuronal networks,[24] direct the differentiation of progenitor and stem cells toward specific neuronal lineages, and facilitate stimulation of differentiated NSCs.[25] During long-term culturing, graphene has been shown to promote hNSC differentiation to neurons upon removal of GF.[26] Recently, graphene foam has been presented as a conducting 3D culture environment and found excellent for growth, differentiation, and electrical stimulation of NSCs.[22]

The fabrication of pyrolysed carbon structures from polymer precursors was pioneered already in the 1970s.[27] Since then, micro-[28–30] and nanometer-sized[29–31] pyrolysed carbon structures have emerged for various applications, for instance, biosensors,[32] microbatteries,[29] cell culture substrates.[33] A number of advantages can be envisaged that make pyrolysed carbon an ideal material for constructing conducting 3D scaffolds for cell and tissue engineering: 1) Organized[29] and random[34] structured scaffolds can be fabricated in a simple process at small or semi-large scale with high reproducibility and high yield as well as cost-effectiveness. Micro/nanostructures can be placed in precisely defined locations without restrictions in shape or cross section and the features and scale depend on the process used for structuring the polymer precursor.[29] 2) By changing the chemical composition of the polymer precursor and pyrolysis conditions, carbon conductivity can be tailored.[28,35] 3) Similarly, the mechanical properties of the scaffold can be tuned[29] to match the stiffness cells experience in vivo.[36] This fabrication flexibility provides possibilities for mass production, facilitating novel custom-made designs with unique properties to support various biomedical and pharmaceutical applications.

Here, we report for the first time fabrication of dense, high-aspect ratio (HAR~8), conducting pillar arrays of pyrolysed carbon, forming 3D scaffolds (p3D-carbon) with pillar diameters approaching the resolution limit of standard UV-lithography. The unique properties of pyrolysed carbon (flat carbon surfaces as control) and the p3D-carbon scaffolds are demonstrated using clinically relevant hNSCs that have been developed for CRT of PD and previously tested in transplantation into a rat model of PD.[4] Even in the presence of GF, without introduction of DF, the pyrolysed carbon induces spontaneous differentiation of hNSCs to dopaminergic neurons with a to date unseen efficiency in both 2D and 3D.[6] We present the first demonstration of electrochemical real-time detection of dopamine exocytosis from populations of hNSC-derived neurons indicating that they have acquired truly dopaminergic phenotype. In the conceptually new approach presented here, the p3D-carbon has three significant functions: 1) Mechanical support for hNSC growth and differentiation, the pillars serving as anchor points for neurites, facilitating formation of neuronal networks. 2) The pyrolysed carbon material itself serves as a next-generation substrate for biomedical devices[37] that not only facilitates but significantly enhances differentiation of hNSCs to dopaminergic neurons. 3) A 3D neurotransmitter trap, enabling electrochemical detection of a larger fraction of the dopamine released by the hNSC-derived neurons than what is possible on conventional 2D electrode substrates (compare the schematic presentation of dopamine detection on 2D and 3D carbon surfaces in **Figure 1**).

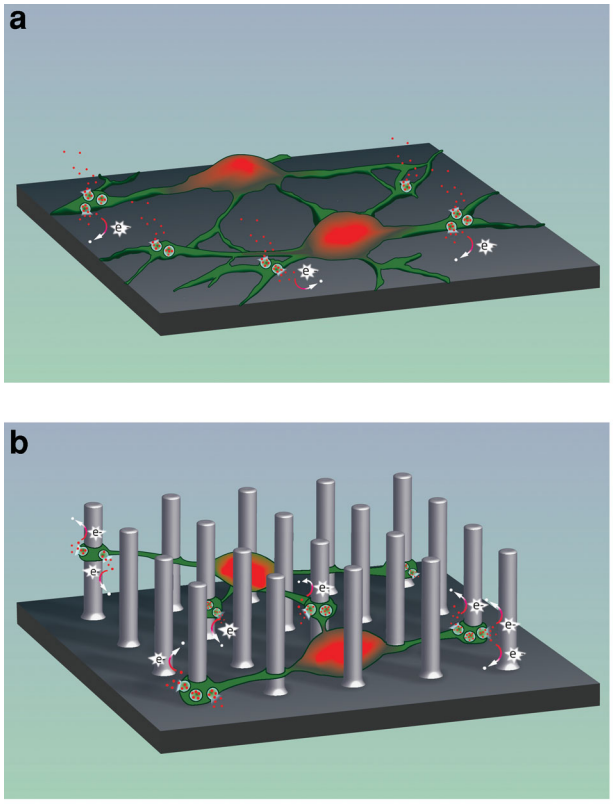

Figure 1. Schematic view of dopamine sensing from hNSCs using pyrolysed carbon structures: a) Traditional measurement mode on a 2D substrate where only a fraction of dopamine reaches the electrode surface and can be detected, while most of the released dopamine diffuses away without being detected. b) New approach using p3D-carbon where the cells differentiate at the bottom or between pillars that therefore function as dopamine traps, allowing detection of a larger fraction of the released dopamine than on a 2D substrate (a).

2. Results and Discussion

2.1. Design and Fabrication of p3D-Carbon

p3D-carbon was fabricated using pyrolysis by carbonizing polymeric micropillar scaffolds patterned in SU-8 (3D-SU8), an epoxy-based negative photoresist. 3D-SU8 (**Figure 2**a) was fabricated using two-step photolithography, involving deposition and crosslinking of a flat SU-8 layer and then patterning a second SU-8 micropillar layer on top (Supporting Information S1), as previously described.[38] During pyrolysis, SU-8 decomposition (gas evolution and aromatization) leads to weight loss and densification,[27] resulting in ≈50% isometric shrinkage of the 3D-SU8 scaffold. The 3D-SU8 was patterned on silicon wafers to form arrays of four scaffolds (each having the foot print of 4 mm × 4 mm) located in the center of chips with dimension 22 mm × 22 mm. 3D-SU8 pillar dimensions were designed to have certain characteristic features: 1) Sufficient pillar height to allow cell growth in a 3D environment within the scaffolds and create a trap for detecting most of the released dopamine. 2) Different pillar diameters and spacings, allowing investigations of how cells migrate, find residence and differentiate with different constraints.

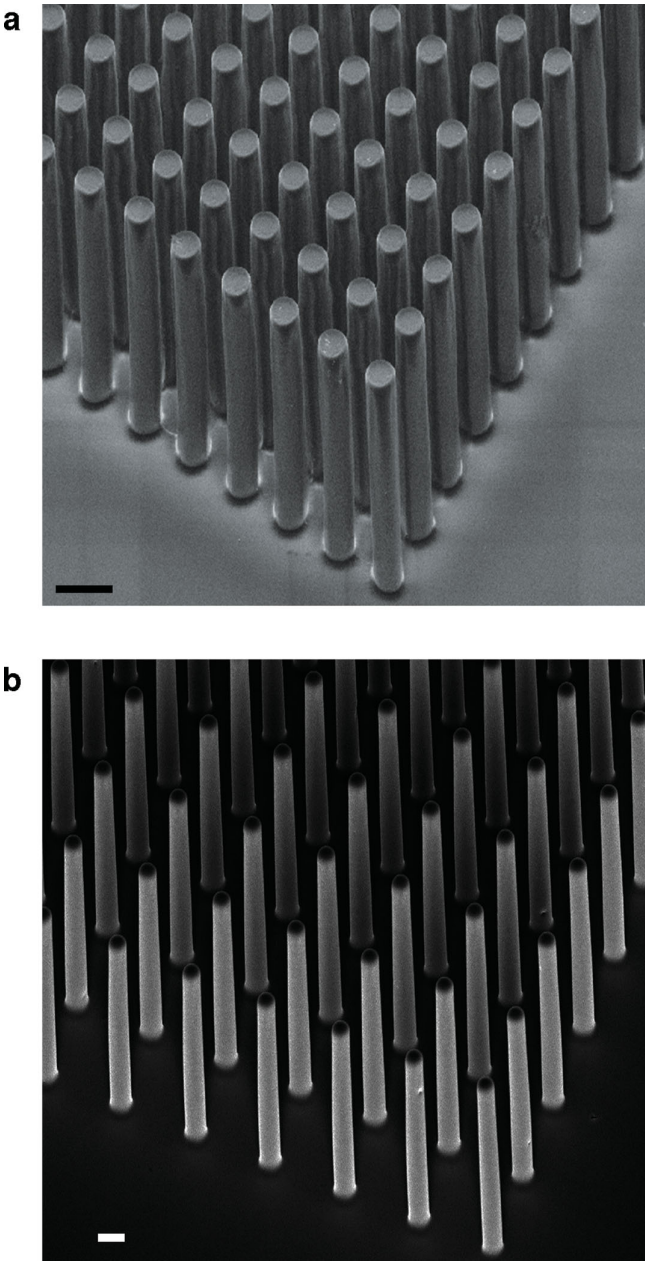

Figure 2. Representative scanning electron microscopic (SEM) images of 3D-scaffolds. a) 3D-SU8 having pillars with 3-μm diameter and 22-μm height. b) p3D-carbon obtained after pyrolysis of the 3D-SU8 in (a). The SU8 pillar diameter and height shrank to 1.4 μm and 11 μm, respectively. The inter-pillar spacing increased from 3 μm to 4.6 μm. Scale bars in (a,b): 5 μm.

2.2. Characterization of Pyrolysed Carbon Surface Properties—Suitability for hNSCs Studies

Wettability, topography and roughness affect behavior of cells on different materials.[39] Cell adhesion, spreading, proliferation and differentiation (e.g., neurite formation) of anchor dependent cells are often less pronounced and delayed on strongly hydrophobic/hydrophilic substrates.[40] Pyrolysed carbon can be functionalized to improve wettability and

biocompatibility.[41,42] Plasma-induced increased wettability has shown to improve neuron adhesion, spreading, and growth,[43] as well as nerve growth factor-induced differentiation of PC12 cells.[40] Here, oxygen plasma-treatment was employed for enhancing wettability of p3D-carbon and flat carbon, followed by characterization of surface chemistry, wettability, as well as adhesion and proliferation of hNSCs.

XPS spectra of untreated and oxygen plasma-treated flat carbon (**Figure 3**a) show a striking increase in oxygen to carbon content ratio (O/C) from 0.022 ± 0.002 to 0.297 ± 0.001 (average ± s.d., $n = 3$), resulting in increased surface energy.[40] The pyrolysed carbon wettability was further investigated using contact angle (CA) measurements (Figure 3b). The CA on untreated p3D-carbon is higher than on flat carbon surfaces (93° ± 2 (1.4-µm pillars), 59° ± 4 (5.1-µm pillars) and 43° ± 1 (flat); average ± s.e.m, $n = 4$), as expected for micropatterns.[43] Plasma treatment dramatically decreases the CA on all structures to values below 20°, indicating increased hydrophilicity

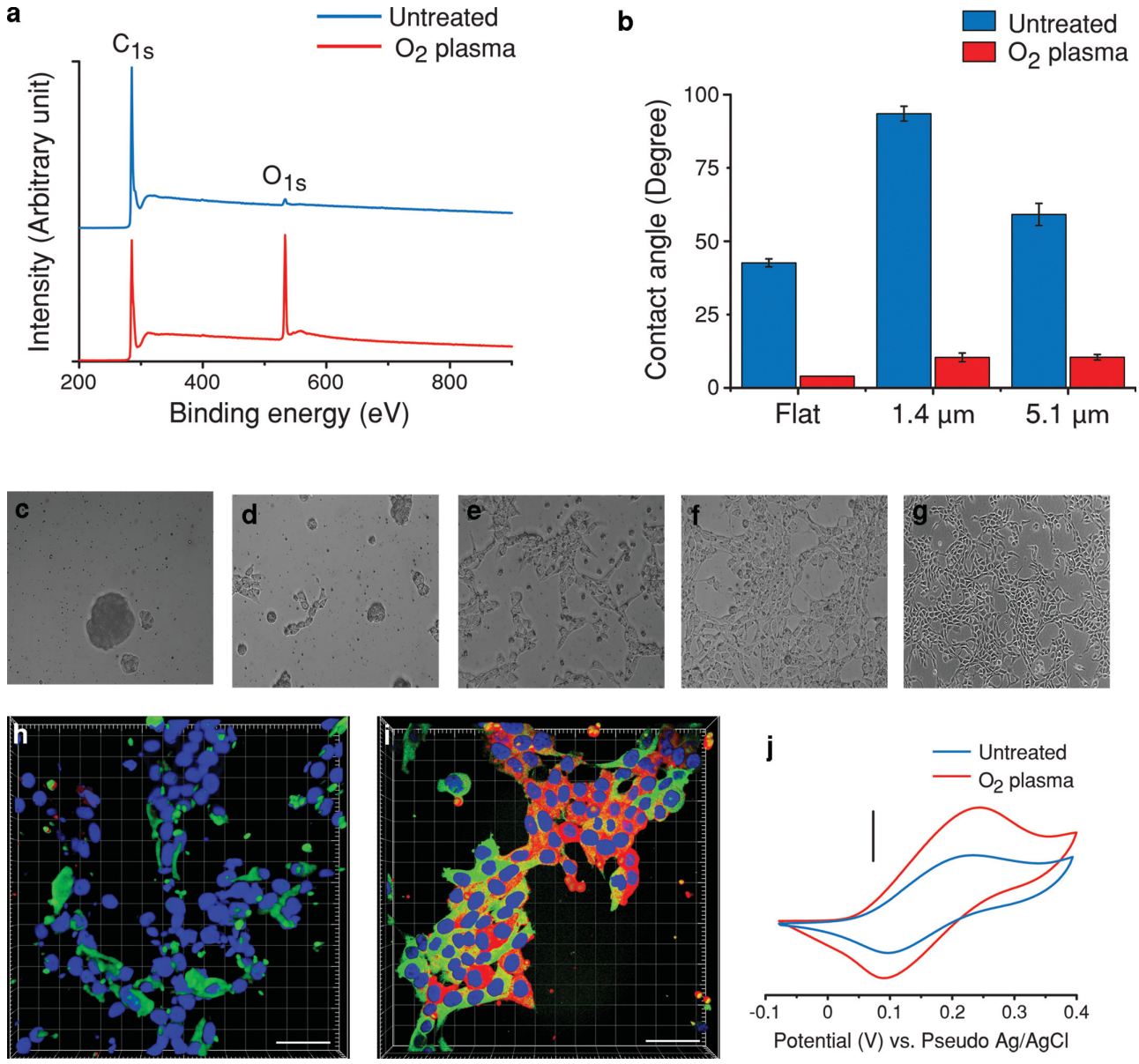

Figure 3. a) Characteristic XPS survey spectra of flat carbon before and after oxygen plasma-treatment. The appearing peaks correspond to C_{1s} (285 eV) and O_{1s} (532 eV). b) Static contact angle measurements on flat carbon (flat) and p3D-carbon (1.4-µm and 5.1-µm pillars). The error bars represent s.e.m.; $n = 4$ for all carbon structures. c–g) Representative bright field images of hNSCs cultured in the presence of growth factors (GF) (48 h) on c) untreated, d) oxygen plasma-treated, e) PLL-coated, f) oxygen plasma-treated and PLL-coated flat carbon surfaces, and g) PLL-coated TCPS. h,i) Representative confocal fluorescence images of immunocytochemistry for tyrosine hydroxylase (red: Alexa Fluor 488), β-tubulin (III) (green: Alexa Fluor 568 goat) and nuclei (blue: TO-PRO-3) in hNSCs cultured in the presence of GF (48 h) on h) PLL-coated TCPS and i) oxygen plasma-treated and PLL-coated flat carbon surfaces. Scale bars in (g,h): 40 µm. j) Characteristic cyclic voltammograms of dopamine (5 mM) in PBS (pH 7) on a p3D-carbon (1.4-µm pillars) before and after oxygen plasma-treatment (V vs Ag/AgCl pseudo-reference electrode; potential sweep rate 50 mV s^{-1}). Scale bar: 5 µA.

(wettability).[44] This is attributed to carbon oxidation rather than increased surface roughness, as AFM imaging indicates (Supporting Information S2).

hNSCs require adhesion factors, for example, poly L-Lysine (PLL), to adhere, grow and differentiate on TCPS.[4] Two types of flat pyrolysed carbon samples (untreated and plasma-treated) were tested with and without PLL-coating for their ability to promote hNSC adhesion, spreading and growth (Figure 3c–f). The results were compared with hNSCs grown on PLL-coated TCPS (Figure 3g). Plasma-treatment combined with PLL-coating is clearly most effective (Figure 3f), resulting in a uniform cell distribution and well-defined cell morphology (compare Figure 3g). Although hNSCs grow well on PLL-coated carbon (Figure 3e), the cell morphology and clustering indicates that PLL adhesion directly on carbon is not optimal. On untreated or plasma-treated (Figure 3d) carbon without PLL, hNSCs adhere poorly, forming clusters without spreading and acquiring proper morphology. Oxygen functionalities after plasma-treatment provide anchoring points for improved physisorption of PLL mediating cell adhesion. This demonstrates that SU-8-derived carbon can easily be modified enabling hNSC studies.

2.3. Dopamine Detection on Pyrolysed Carbon Structures: Flat Carbon vs p3D-Carbon

2.3.1. Dopamine Electrochemistry

Despite the differences in conductivity, various carbon materials have been used for dopamine electrochemistry, for example, nitrogen-doped diamond-like carbon (9.4×10^{-3} Ω m),[45] boron-doped diamond[46] ($0.5–1.0 \times 10^{-3}$ Ω m),[47] glassy carbon[48] (GC) ($1–8 \times 10^{-5}$ Ω m),[49] and basal plane graphite[46] ($2.5–5.0 \times 10^{-6}$ Ω m).[50] The electrical properties of pyrolysed carbon depend on many parameters, including viscoelasticity and chemical composition of the precursor polymer,[35] fabrication method,[29] as well as pyrolysis temperature[35,51,52] and atmosphere.[51] In our study, the resistivity of the pyrolysed carbon was found to be $1.6 \pm 0.3 \times 10^{-4}$ Ω m (average ± s.e.m., $n = 9$), similarly as previously reported for carbonized SU-8 ($5–7 \times 10^{-4}$ Ω m).[52] As shown previously, dopamine detection can be performed on different carbon electrode materials having varying degree of conductivity affecting the kinetics.[46]

As shown above (Section 2.2), SU-8-derived carbon requires oxygen plasma-treatment in preparation for hNSC applications. Due to this, we specifically characterized the behavior of dopamine electrochemistry before and after oxygen plasma-treatment. Cyclic voltammetry (CV) was used to investigate dopamine electrochemistry on flat carbon and p3D-carbon. Figure 3j shows CVs for p3D-carbon (1.4-µm pillars). The redox behavior is quasi-reversible before and after plasma treatment. However, both anodic and cathodic peak current clearly increased after plasma-treatment. Similar results were obtained for both flat- and p3D-carbon (5.1-µm pillars). The observed current increase can be explained by: 1) Optimal orientation of electroactive OH-groups of dopamine is mediated by the hydrogen bonding capability of carbonyl and carboxyl functionalities at plasma-treated carbon surfaces, thereby improving the sensitivity for dopamine similarly as described for chemically modified metal electrodes[12,14,53] and GC with hydrogen bonding sites.[48] 2) The effect of plasma-treatment is more substantial on p3D-carbon compared to flat carbon (result not shown). This is attributed to increased exposure of the pillar surface to dopamine due to enhanced wettability. This demonstrates that SU-8-derived p3D-carbon is suitable for dopamine electrochemistry.

2.3.2. Monitoring of Dopamine Exocytosis from Cell Populations

The suitability of p3D-carbon for monitoring dopamine exocytosis from populations of growing and differentiating cells was first investigated using PC12 cells. Growth (24 h) and differentiation (120 h) of PC12 cells were performed in parallel on oxygen plasma-treated and laminin-coated chips with different carbon structures (flat carbon and p3D-arbon). An individual cell population was cultured in each of the four quadrants of a chip having the footprint of 4 mm × 4 mm (Supporting Information S5 and S6). **Figure 4**a shows a typical current-time

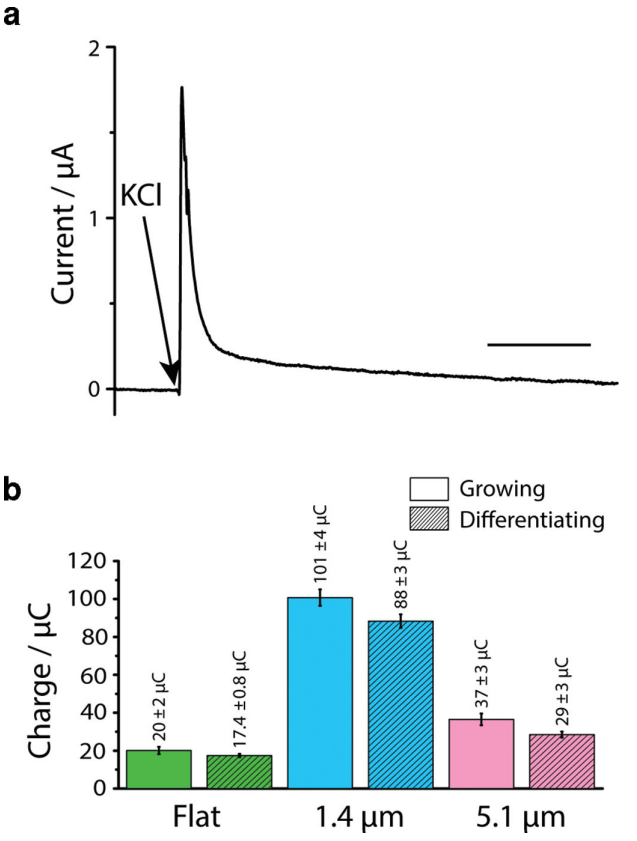

Figure 4. a) A characteristic current-time trace recorded during amperometric detection of dopamine released by a population of growing PC12 cells on oxygen plasma-treated and laminin modified flat carbon, when the cells were depolarized by elevated K^+ concentration. Time scale bar, 1 min. The arrow indicates the time of addition of high-K^+ buffer (KCl). b) Calculated average charge related to the amount of detected dopamine released by growing (24 h) and differentiating PC12 cells (120 h) on flat carbon surfaces and p3D-carbon (1.4-µm and 5.1-µm pillars). Error bars represent s.e.m.; $n = 4$ for flat carbon surfaces and n = 6 for each type of the p3D-carbon.

trace recorded during K^+-induced dopamine exocytosis from a population of growing PC12 cells. The current represents the sum of responses related to oxidation of dopamine released from individual fusing vesicles upon membrane depolarization. Performed control experiments clearly show that the recorded current is not caused by ionic current artefacts due to fluid addition or cell movement on the carbon surfaces (Supporting Information S4).

Similarly to the current originating from single-cell exocytosis measurements,[54] the amount of signaling substance (ultimately number of molecules) detected/released by a cell population can be determined by integrating the recorded current.[14] The results for populations of growing and differentiating PC12 cells (Figure 4b) show clear trends. The average charge is significantly higher for 1) p3D-carbon than for flat carbon surfaces, 1.4-µm pillars yielding the highest charge, and 2) for growing PC12 cells compared to differentiating cells irrespective of carbon topography. Although the p3D-carbon has larger surface area compared to flat carbon (for 5.1-µm and 1.4-µm pillars the increase in surface area is 1.6- and 1.9-fold, respectively), it does not explain the first trend, that is, the higher electrochemical response, since the cell population on the different carbon structures had the same number of cells. It is more likely that the p3D-carbon serves as an efficient dopamine trap. When dopamine is released in a p3D-carbon scaffold, the molecules encounter the surrounding carbon pillars (Figure 1b), leading to oxidation of a larger number of molecules than on flat carbon where most of the molecules diffuse away without being detected (Figure 1a). This effect is more pronounced for the 1.4-µm pillars due the more densely structured scaffold, that is, less distance between pillars, and higher likelihood that a dopamine molecule will encounter a pillar and be oxidized. The second trend is in accordance with previous reports[10,55] and is due to the change in location of the exocytotic zones in differentiating PC12 cells (from the cell body to the neurite-like structures). The above results demonstrate that the p3D-carbon, aside from being suitable for detection of exocytotic events and discriminating biological differences between cell populations, provides a significantly more efficient detection possibility due to the 3D environment.

2.4. Influence of Pyrolysed Carbon Structures on hNSCs

Previous studies, using microtowers (250 µm high and 200 µm in diameter)[18] and micropillars (10 µm high and 10 µm in diameter)[19] to define a 3D environment for neuronal cultures, have shown the enhancement of neurite growth and formation of neuronal networks. Graphene was shown to promote differentiation of hNSCs to neurons when GF (fibroblast growth factor, FGF; epidermal growth factor, EGF) were removed from the medium.[26] In our study, the goal was to direct the fate of hNSCs to dopaminergic neurons. In order to differentiate between the possible effect of pyrolysed carbon itself and the 3D environment provided by the p3D-carbon, the behavior of hNSCs was first characterized on flat pyrolysed carbon surfaces and compared with cells on TCPS.

2.4.1. Influence of Pyrolysed Carbon Material

Indirect means are usually used to confirm neural and dopaminergic phenotype of differentiated hNSCs, such as ICC for tyrosine hydroxylase (TH; the rate-limiting enzyme for catecholamine synthesis) and β-tubulin (III) (an indicator of neural cytoskeleton development).[4,5,56] Previously, for the hNSCs studied here, the highest obtained percentage of TH-positive (TH^+) cells without and with DF was ≈2 and 17–18% on PLL-coated TCPS, respectively.[4,5] A recent report indicates that pyrolysed carbon seems to enhance neurite outgrowth of neuroblastoma cells.[33] Here, the influence of pyrolysed carbon on dopaminergic properties of hNSCs was initially characterized using ICC for TH and β-tubulin (III). hNSCs were cultured for 48 h in the presence of GF on oxygen plasma-treated PLL-coated flat carbon to see if the carbon material itself has any ability to induce dopaminergic properties in hNCSs without introducing DF. hNSCs cultured on PLL-coated TCPS were used as control. Figure 3 shows confocal fluorescence images of hNSCs cultured on TCPS (h) and on carbon (i). Cell growth on carbon is accompanied by a previously unseen increase in the percentage of TH^+ cells to 75 ± 9% as compared with 2.5 ± 0.6% on PLL-coated TCPS (average ± s.d., $n = 5$; Supporting Information S3). Moreover, the presence of β-tubulin (III) is more pronounced in cells growing on carbon. The result clearly indicates that pyrolysed carbon rapidly induces spontaneous differentiation of hNSCs even when the cells are cultured in the presence of GF unlike, for instance, graphene which induces differentiation of hNSCs during long-term culturing after removal of GF.[26] Our result may have important implications for finding new materials and improved protocols for effective implementation of CRT as a treatment for PD.

2.4.2. Influence of the 3D Environment of p3D-Carbon

In order to evaluate the influence of the 3D environment of p3D-carbon on differentiation of hNSCs, especially in terms of dopaminergic properties, we expanded the initial experimental study presented above (Section 2.4.1.) to include culturing in the presence of DF. The influence of pyrolysed carbon material (flat structures) was compared to that of p3D-carbon using a combination of SEM and confocal fluorescence imaging (ICC for TH and counterstaining of nuclei). SEM images in **Figure 5**b-c show hNSCs cultured for 48 h in the presence of GF on the different p3D-carbon structures. The pillar topography clearly leads to formation of elongated neurites, which are using the pillars as anchoring points. These elongated neurites are not observed on flat carbon (Figure 5a). Confocal images, on the other hand, show that the hNSCs growing in the absence of differentiation inducing conditions effectively become TH^+ (75–82%; details in Supporting Information S3) on all surfaces (Figure 5d–f).

Comparing SEM images of hNSCs cultured in the presence of GF (Figures 5a–c) and DF (Figures 5g–i), the neurite elongation is in all cases more prominent after hNSCs have been exposed to DF, and most significantly so for the 1.4-µm pillars. Visual inspection of confocal images (Figure 5j–m)

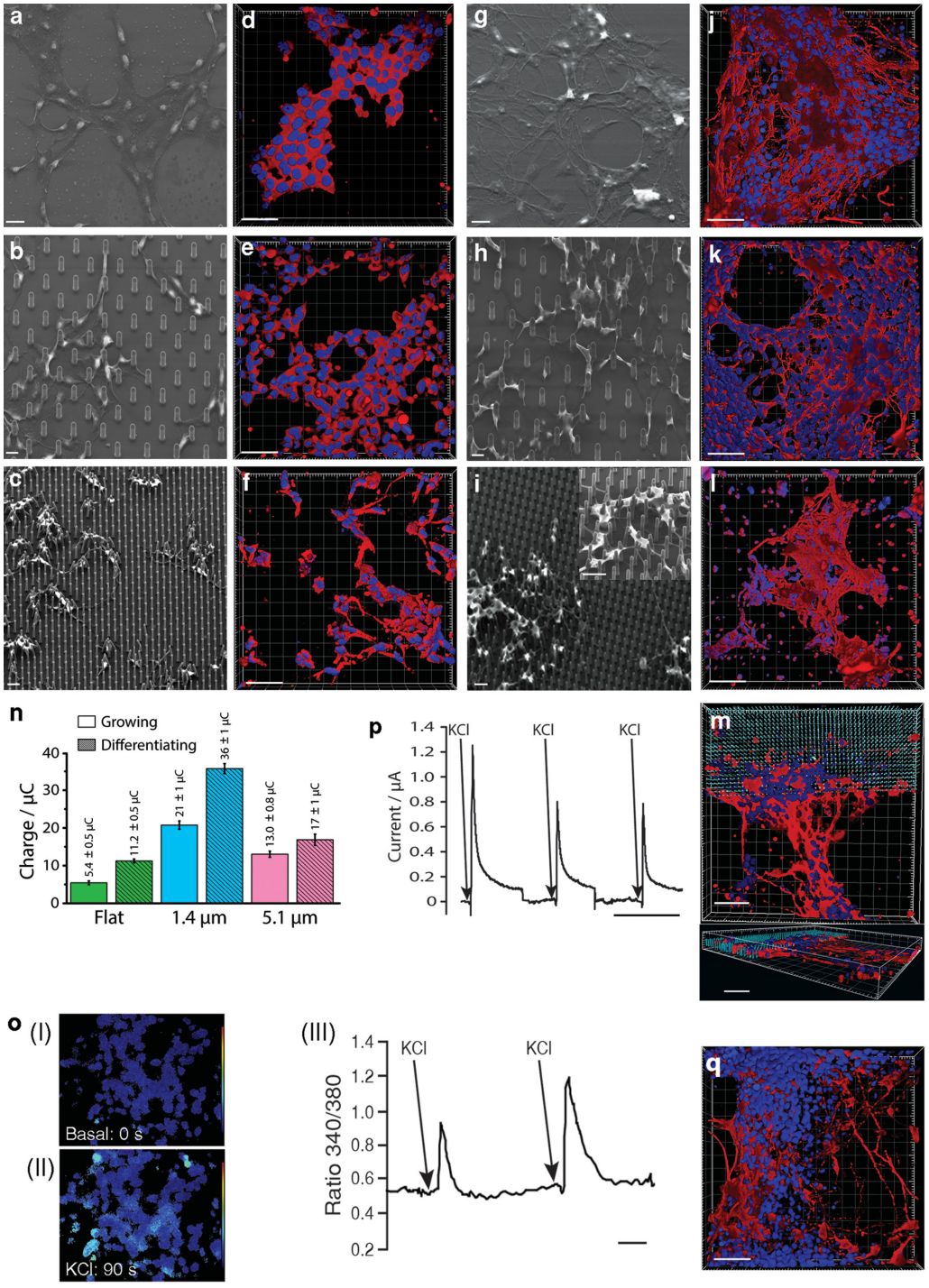

Figure 5. Characterization hNSCs cultured in the presence of growth factors (GF-conditions; 48 h) and differentiation factors (DF-conditions; 10 days): a–c,g–i) Representative SEM images for GF- (a–c) and DF-conditions (g–i) on flat carbon (a,g), 5.1-µm (b,h), and 1.4-µm (c,i) p3D-carbon. Inset of (i): magnification of hNSCs interacting with carbon pillars. Scale bars: 20 µm (a,g) and 10 µm (b,c,h,i,inset of i). d-f,j-m,q) Representative confocal fluorescence images showing immunocytochemistry of tyrosine hydroxylase (red: Alexa Fluor 488), and counterstaining of nuclei (blue: TO-PRO-3) for GF- (d–f) and DF-conditions (j–m,q) on flat carbon (d,j), 5.1-µm (e,k), and 1.4-µm (f,l,m) p3D-carbon as well as on TCPS (q). Scale bars, 40 µm (d–f,j–l,q), 50 µm (m). n) Calculated average charge related to the amount of detected dopamine released by hNSCs GF- and DF-conditions on flat carbon surfaces and p3D-carbon (1.4-µm and 5.1-µm pillars). Error bars represent the standard error of mean, $n = 4$ for the flat carbon surfaces and $n = 6$ for each type of p3D-carbon. o) Representative confocal fluorescence images of cytosolic Ca^{+} in hNSCs under DF-conditions (basal level, I; depolarized cells, II). III) Changes in Ca^{2+} level are shown as the fluorescence intensity ratio at 340 nm and 380 nm excitation. The arrows indicate the time of addition of high-K^{+} buffer (KCl). p) Characteristic current-time trace recorded during amperometric detection of dopamine from a population hNSCs under DF-conditions on a flat carbon surface upon multiple K^{+}-induced depolarization steps. The arrows indicate the time of addition of high-K^{+} buffer (KCl). Time scale bar (o-III, p), 2 min.

of cells exposed to DF (Figure 5m shows hNSCs at the interface between 1.4-μm pillar scaffold and the surrounding flat carbon surface illustrating the distinction between cells in a 3D environment and on a flat surface; upper panel: top view, lower panel: *xz*/*yz*-plane) indicates that the number of TH^+ cells has increased compared to cells without introduced DF (Figures 5d–f). This can be explained by the fact that the total number of cells has increased since the proliferation of hNSCs does not completely stop during the first few days of differentiation, which is in accordance with previous studies.[56] However, the cell population means of TH^+ hNSCs exposed to DF (73–75%) was found not to be statistically different from cells cultured in the absence of DF (two-way ANOVA, $\alpha = 0.05$, $p = 0.163$; details in Supporting Information S3). This can be compared to 24 ± 2% (average ± s.d., $n = 5$) of TH^+ hNSCs on TCPS in the presence of DF (Figure 5q). These observations confirm that the carbon material definitely induces dopaminergic properties and show that the primary effect of 3D environment seems to be an enhancement of neurite elongation and formation of neuronal networks, which is in accordance with the presented findings on neuronal cultures using 3D environment of microtowers[18] and micropillars.[19] Moreover, the results show that pyrolysed carbon material in combination with 3D environment induces differentiation of hNSCs to dopaminergic neurons with a twofold efficiency than previously shown for differentiation of rodent stem cells in 3D peptide nanowire scaffolds to dopaminergic phenotype.[6]

2.4.3. Characterization of the Dopaminergic Properties: the Exocytotic Function

The studied hNSCs produce only dopamine since they do not express the enzyme dopamine-beta-hydroxylase, which is needed for transition into the noradrenergic and adrenergic pathways.[56] Since the purpose is to determine the fate of an entire cell population, whose evaluation with exocytosis measurements is statistically significant,[57] single-cell measurements with, for example, CFMEs, are not applicable in this study. Here, we show amperometric detection of the released dopamine from depolarized hNSCs cultured in the presence of GF and DF (presented as the charge in Figure 5n). Similarly as for the PC12 cell experiments (Figure 4b), the results clearly demonstrate that the 1.4–μm pillar p3D-carbon functions as a very efficient dopamine trap. We also see that on all surfaces cells have clearly acquired the capability of exocytotic dopamine release even when the cells were cultured in the presence of GF. The apparently higher charge obtained for differentiated hNSCs on all structures can have two explanations: 1) The most apparent reason is that the imposed differentiation conditions increase the cells' ability to exocytotically release dopamine. 2) The fact that the cells continue proliferation during the first few days of exposure to DF[56] means that the total number of cells increases and thus a larger quantity of dopamine can be released. To differentiate between the significance of these two contributions, further studies will be conducted involving methods that readily facilitate cell quantitation in a 3D environment (e.g., DNA based quantitation).

Mature neurons have the ability to reestablish the resting membrane potential and close the voltage-gated Ca^{2+} channels after K^+-induced depolarization,[56] that is, they are able to undergo repetitive depolarization. This cellular property is traditionally verified by fluorescence microscopic imaging of Ca^{2+} influx, as seen in Figure 5o for hNSCs differentiated on PLL-coated TCPS. However, this is a characteristic feature of all neurons undergoing exocytosis, not only dopaminergic neurons.[56] In Figure 5p, the effect of repetitive depolarization of hNSCs differentiated on flat carbon is demonstrated using electrochemical detection, verifying that the dopaminergic hNSCs have become mature neurons, each depolarization step leading to dopamine release. Immunocytochemistry gives indirect information that hNSCs develop into dopaminergic phenotype (TH^+), and Ca^{2+} imaging indicates that they become mature neurons. However, neither method provides proof of the ability to exocytotically release dopamine or that dopamine releasing cells are mature dopaminergic neurons. This is only possible by electrochemical real-time detection, which is demonstrated to be more efficient in the 3D environment of p3D-carbon in comparison with 2D electrodes.

3. Conclusions

We have shown fabrication of pyrolysed carbon 3D scaffolds (p3D-carbon) dimensionally reaching the limit of UV lithography. Application of the p3D-carbon scaffolds for differentiation of human neural stem cells (hNSCs) demonstrates the uniqueness of pyrolysed carbon as a material. It rapidly induces spontaneous differentiation of hNSCs to dopaminergic neurons even under conditions that conventionally are used for hNSC proliferation while differentiation is suppressed. Moreover, the 3D environment clearly enhances elongation of neurites and formation of neuronal networks. The conductivity of the pyrolysed carbon enables electrochemical real-time detection of dopamine exocytosis from populations of hNSC-derived neurons, which is to date the first demonstration of such measurements on hNSCs. The results provide the ultimate confirmation of the true dopaminergic phenotype and maturation. The 3D environment of the p3D-carbon shows an enhanced efficiency in dopamine detection (dopamine trap), being able to detect a larger fraction of the released dopamine in comparison with 2D electrodes. This work represents a new direction in hNSC research and opens up new possibilities for construction of scaffolds useful in cell replacement therapy of Parkinson's disease, and generally in neuronal regeneration related to central nervous system injuries, as well as implantable electrodes for deep brain stimulation and neurotransmitter monitoring. Our unique findings warrant further studies on the effect of pyrolysed carbon as material derived from different polymeric precursors in combination with 3D environment on the molecular level behavior of hNSC differentiation.

4. Experimental Section

Reagents: Potassium chloride, sodium hydroxide, glucose (BioXtra), sodium chloride, magnesium chloride hexahydrate, calcium chloride

dihydrate, 4-(2-hydroxyethyl)piperazine-1-ethanesulfonic acid (HEPES, 1 M), and formaldehyde (36% in water) (BioReagent), glutaraldehyde (25% in water for electron microscopy), 2-(3,4-dihydroxyphenyl) ethylamine hydrochloride (Dopamine), L-3,4-dihydroxyphenylalanine (L-DOPA), cell culture tested water, phosphate buffered saline (PBS), poly L-lysine hydrobromide (PLL: Mw 70 000–150 000 kDa; BioXtra), laminin from Engelbreth-Holm-Swarm murine sarcoma basement membrane, Triton X-100 (10% in water; BioUltra), goat serum, monoclonal mouse anti-tyrosine hydroxylase antibody (anti-TH), and polyclonal rabbit anti-β-tubulin (III) antibody (anti-β-tubulin) were purchased from Sigma-Aldrich Corporation (St. Louis, MO, USA). Alexa Fluor 488 goat anti-mouse IgG antibody, Alexa Fluor 568 goat anti-rabbit IgG antibody, and TO-PRO-3 stain were from Life Technologies Ltd. (Paisley, UK). 96% ethanol and absolute ethanol were from Kemetyl A/S (Køge, Denmark).

Pyrolysis: SU-8 structures were pyrolysed in a PEO-601 furnace from ATV Technologie GmbH (Vaterstetten, Germany) under nitrogen atmosphere. The protocol comprised three stages: i) Temperature ramping from room temperature (RT) to 200 °C followed by 30-min dwelling time to allow removal of residual oxygen (prevention of combustion at higher temperatures). ii) Temperature ramping from 200 °C to 900 °C followed by 1-h dwelling time to complete carbonization. iii) Cooling down to RT. Temperature ramping during heating and cooling was done at the rate of 2 °C/min.

Electric Contacts: Preparation of gold coated electric contacts for pyrolysed carbon is described in Supporting Information (S5).

Scanning Electron Microscopic Characterization: Imaging of carbon structures and growing/differentiating cells was done using a Zeiss Supra VP 40 microscope. Cells were fixed for 1 hour in 2% glutaraldehyde (diluted in PBS), rinsed twice with PBS (15 min) and water (5 min). Dehydration of cell chips was performed exposing them to a series of ethanol-water solutions (40% to 100%; absolute ethanol).

O_2 Plasma-Treatment: Carbon structures were modified with O_2 plasma using a 13.56 MHz RF generator-equipped Atto Plasma System (Diener Electronic GmbH, Ebhausen, Germany). The chamber was evacuated initially to a pressure below 15 Pa, after which O_2 was introduced (pressure stabilization at 30 Pa) and the plasma was ignited (power 50 W, duration 1 min). Immediately after plasma-treatment, carbon structures were used for surface characterization or cell culture experiments.

Resistance Measurements: Four-point probe resistance measurements (lock-in technique) of pyrolysed carbon were performed using a CAPRES microRSP-M150 system with static contact microscopic probe (M4PP). The current set-point and frequency were 200 µA and 13 Hz, respectively. All measurements showed phase change of less than 0.2 degree. The result of resistance measurements is presented as average ± s.e.m., n being the total number of analyzed positions on different carbon surfaces.

X-Ray Photoelectron Spectroscopic (XPS) Analysis: The carbon surfaces were analyzed using a K-Alpha spectrometer (Thermo Fisher Scientific, UK) with monochromatized 400-µm AlKa X-ray spot (pass energy: 200 eV for survey spectra). Analysis was conducted before and immediately after plasma-treatment. The Avantage software package (v4.84) facilitated elemental composition analysis. All the results of elemental composition analysis are presented as average ± s.d. ($n = 3$).

Contact Angle (CA) Measurements: Static CA at the carbon structures was measured with water as the wetting agent (2-µL drop) before and immediately after plasma-treatment using an OCA 20 goniometer controlled by SCA-20 software package (DataPhysics Instruments GmbH, Filderstadt, Germany). All the results of CA measurements are presented as average ± s.e.m., *n* being the total number of analyzed positions on different carbon structures.

Dopamine Electrochemistry on Carbon Structures: 5 mM dopamine solutions for cyclic voltammetric (CV) characterization were prepared immediately before use in nitrogen purged PBS (20 min). The CVs were acquired using a micromilled poly(methyl methacrylate) (PMMA) chip holder (Supporting Information S6), having a 70-µL vial for each quadrant of the silicon chip with carbon structures (Supporting Information S5). Electric connections to the potentiostat (CHI 1030 from CH Instruments Inc., Austin TX, USA) were formed as described in the Supporting Information (S5 and S6). An Ag/AgCl wire and a Pt wire were used as the pseudo reference electrode (RE) and counter electrode (CE), respectively.

Culturing of Rat Pheochromocytoma (PC12) Cells: PC12 cells were grown and differentiated as described elsewhere[14] (details in Supporting Information S7).

Culturing of Human Neural Stem Cells (hNSCs): Cells from the immortalized human ventral mesencephalic cell line overexpressing Bcl-XL (hVM-Bcl-XL) were cultured as described elsewhere[4,5] (details in Supporting Information S8).

Preparation of Carbon Structures for Cell-based Experiments: The silicon chips with carbon structures (Supporting Information S5) were oxygen plasma-treated unless otherwise stated. The chips and chip holders (Supporting Information S6) were sterilized by immersion in 96% ethanol (10 min) and 0.5 M NaOH (30 min), respectively, followed by rinsing three times with PBS and coating with laminin (20 mg/mL in PBS, 3 h; for PC12 cells) or PLL (10 µg/mL in PBS; 3 h; for hNSCs) to promote cell adhesion. Cells were seeded onto the coated electrode chips at the density 150 000 cells/cm^2 (PC12 cells) and 30 000 cells/cm^2 (hNSCs). Chips with different carbon structures (flat surfaces and p3D-carbon scaffolds) were prepared in parallel for all experimental conditions (SEM imaging, immunocytochemistry with confocal microscopic imaging and electrochemical exocytosis measurements).

Exocytosis Measurements: The low-K^+ buffer (10 mM HEPES, 5 mM glucose, 1.2 mM $MgCl_2$, 2 mM $CaCl_2$, 150 mM NaCl, and 5 mM KCl), and high-K^+ buffer (same as low K^+ buffer but 5 mM Na^+ and 450 mM K^+) were sterile filtered (0.2-µm syringe filter). Fluid additions during measurements were facilitated using the open vial of the chip holder. Before exocytosis measurements, a baseline current was recorded in 55 µL of the low-K^+ buffer. Two platinum wires served as RE and CE. The carbon-working electrode (WE) was poised at 350 mV vs RE. After recording a stable baseline, exocytosis was triggered by pipetting 15 µL of the high-K^+ buffer directly into the vial to elevate the K^+ concentration to 100 mM. The current–time traces corresponding to the released dopamine were obtained immediately after triggering exocytosis. Exocytotic events were recorded in each quadrant of the silicon chips with carbon structures (Supporting Information S5). The amperometric recordings were performed at room temperature (RT; ≈22 °C) using a CHI 1030 potentiostat. Integration of the recorded current was performed using the function provided in the software of CHI electrochemical analyzer (v. 8.17) by the manufacturer CH Instruments. The *i–t* curves were integrated in the time interval of 60 s for all conditions and carbon structures (flat and p3D-carbon). The results are presented as average ± s.e.m. (n = total number of different carbon structures having a cell population). The dopamine load in PC12 cells was increased by 1-h incubation in fresh medium containing 100 µM L-DOPA before the measurements.[14]

Live-Cell Ca^{2+} Imaging: Ca^{2+} influx studies were performed as described elsewhere[7] (details in Supporting Information S9).

Immunocytochemistry and Confocal Microscopy: Cells were fixed for 15 min at RT in 4% formaldehyde (in PBS) followed by rinsing with PBS (three times for 5 min). To permeabilize cell membranes and block unspecific binding of antibodies, the fixed cells were incubated at RT for 1 h in PBS containing 10% goat serum and 0.25% Triton X-100. After removal of the blocking solution, the cells were incubated with primary antibodies (anti-TH and anti-β-tubulin; both diluted 1:1000 in PBS containing 1% goat serum and 0.25% Triton X-100) overnight at 4 °C followed by rinsing for 10 min in each of the rinsing solutions (1° PBS containing 1% goat serum and 0.25% Triton X-100; 2° PBS containing 0.25% Triton X-100; 3° PBS). Incubation with secondary antibodies (anti-mouse and anti-rabbit; both diluted 1:200 as described for primary antibodies) was done at RT for 30 min followed by rinsing with PBS (twice for 10 min). Cell nuclei were counterstained with TO-PRO-3 (diluted 1:500 in PBS) for 10 min followed by rinsing in PBS (three times for 10 min) and water (5 min). Confocal laser scanning microscopy was performed using a Leica TCS SP5 microscope (Leica Microsystems,

Wetzlar, Germany) equipped with a 50×/0.75 W objective. Five images were acquired from each prepared cell population on a carbon chip or TCPS (randomly chosen locations). A 488-nm Ar laser, 543-nm HeNe laser, and 633-nm HeNe laser was used for exciting Alexa Fluor 488, Alexa Fluor 568, and TOPRO-3, respectively. All the acquired images were analyzed and treated using Imaris software package (v7.4.2) (Bitplane AG, Zürich, Switzerland).

Percentage of TH-Positive (%TH$^+$) hNSCs: To determine%TH$^+$ hNSCs in a population, the cells were counted after immunocytochemistry and confocal microscopic imaging as described above for TH and nuclei (to yield the total number of cells). Cells in the five representative images acquired for each population on a carbon chip or TCPS were counted using Imaris software package. Each image comprised a *z*-stack with dimension of 20–25 μm (the thickness of each plane was 0.6 μm). All the calculated values of%TH$^+$ are presented as average ± s.d. ($n = 5$).

Statistical Analysis: Statistical comparison of%TH$^+$ hNSCs in populations of growing and differentiating cells on different carbon structures was performed using two-way ANOVA ($\alpha = 0.05$) function in Origin (v8.6) (OriginLab Corporation, Northampton, MA, USA). p values < 0.05 were considered statistically significant. Variances in all compared populations were statistically similar. Additional details of the statistical analysis are described in the Supporting Information (S3).

Supporting Information

Supporting Information is available from the Wiley Online Library or from the author.

Acknowledgments

A.H. acknowledges Ørsted postdoctoral fellowship and Lundbeck Foundation (R69-A6408) for financial support. A.M.S. acknowledges financial support from EU (NMP-SL-2008–214706, EXCELL), MINECO (PLE2009–0101 and SAF2010–17167), TerCel (RD12/0019/0013), Neurostem-CM (S2010-BMD-2336), and institutional grant from Fundación Ramón Areces to the CBMSO. Nanna Bild from DTU Nanotech is acknowledged for the artwork in Figure 1.

Received: March 12, 2014
Revised: June 17, 2014
Published online: September 11, 2014

[1] M. Politis, O. Lindvall, *BMC Med.* **2012**, *10*, 1.
[2] A. K. Meyer, M. Maisel, A. Hermann, K. Stirl, A. Storch, *J. Neurol. Sci.* **2010**, *289*, 93.
[3] C. Perrone-Capano, U. Di Porzio, *Int. J. Dev. Biol.* **2000**, *44*, 679.
[4] E. T. Courtois, C. G. Castillo, E. G. Seiz, M. Ramos, C. Bueno, I. Liste, A. Martínez-Serrano, *J. Biol. Chem.* **2010**, *285*, 9881.
[5] C. Krabbe, E. Courtois, P. Jensen, J. R. Jørgensen, J. Zimmer, A. Martínez-Serrano, M. Meyer, *J. Neurochem.* **2009**, *110*, 1908.
[6] N. Ni, Y. Hu, H. Ren, C. Luo, P. Li, J.-B. Wan, H. Su, *PLoS One* **2013**, *8*, e84504.
[7] J. Tønnesen, E. Gonzalez Seiz, M. Ramos, O. Lindvall, A. Martinez-Serrano, M. Kokaia, *Exp. Neurol.* **2010**, *223*, 653.
[8] A. G. Westerink, R. H. Ewing, *Acta Physiol.* **2008**, *192*, 273.
[9] R. M. Wightman, J. A. Jankowski, R. T. Kennedy, K. T. Kawagoe, T. J. Schroeder, D. J. Leszczyszyn, J. A. Near, E. J. Diliberto, O. H. Viveros, *Proc. Natl. Acad. Sci. U.S.A.* **1991**, *88*, 10754.
[10] S. Zerby, A. G. Ewing, *Brain Res.* **1996**, *712*, 1.
[11] A. F. Dias, G. Dernick, V. Valero, M. G. Yong, C. D. James, H. G. Craighead, M. Lindau, *Nanotechnology* **2002**, *13*, 285.
[12] C. Spégel, A. Heiskanen, J. Acklid, A. Wolff, R. Taboryski, J. Emnéus, T. Ruzgas, *Electroanalysis* **2007**, *19*, 263.
[13] X. Liu, S. Barizuddin, W. Shin, C. J. Mathai, S. Gangopadhyay, K. D. Gillis, *Anal. Chem.* **2011**, *83*, 2445.
[14] L. Sasso, A. Heiskanen, F. Diazzi, M. Dimaki, J. Castillo-León, M. Vergani, E. Landini, R. Raiteri, G. Ferrari, M. Carminati, M. Sampietro, W. E. Svendsen, J. Emnéus, *Analyst* **2013**, *138*, 3651.
[15] P. Zorlutuna, N. Annabi, G. Camci-Unal, M. Nikkhah, J. M. Cha, J. W. Nichol, A. Manbachi, H. Bae, S. Chen, A. Khademhosseini, *Adv. Mater.* **2012**, *24*, 1782.
[16] E. Carletti, A. Motta, C. Migliaresi, in 3D Cell Culture: Methods and Protocols, *Methods in Molecular Biology* (Ed: J. W. Haycock), Springer Science+Business Media, New York, USA **2011**, 17–39.
[17] F. Pampaloni, E. G. Reynaud, E. H. K. Stelzer, *Nat. Rev. Mol. Cell Biol.* **2007**, *8*, 839.
[18] D. K. Cullen, J. A. Wolf, V. N. Vernekar, J. Vukasinovic, M. C. LaPlaca, *Crit. Rev. Biomed. Eng.* **2011**, *39*, 201.
[19] T. Limongi, F. Cesca, F. Gentile, R. Marotta, R. Ruffilli, A. Barberis, M. Dal Maschio, E. M. Petrini, S. Santoriello, F. Benfenati, E. Di Fabrizio, *Small* **2013**, *9*, 402.
[20] S.-Z. Yow, T. H. Lim, E. K. F. Yim, C. T. Lim, K. W. Leong, *Polymers* **2011**, *3*, 527.
[21] S. R. Shin, S. M. Jung, M. Zalabany, K. Kim, P. Zorlutuna, S. Kim, M. Nikkhah, M. Khabiry, M. Azize, J. Kong, K. Wan, T. Palacios, M. R. Dokmeci, H. Bae, X. Tang, A. Khademhosseini, *ACS Nano* **2013**, *7*, 2369.
[22] N. Li, Q. Zhang, S. Gao, Q. Song, R. Huang, L. Wang, L. Liu, J. Dai, M. Tang, G. Cheng, *Nat. Sci. Rep.* **2013**, *3*, 1.
[23] M. R. Abidian, E. D. Daneshvar, B. M. Egeland, D. R. Kipke, P. S. Cederna, M. G. Urbanchek, *Adv. Healthcare Mater.* **2012**, *1*, 762.
[24] V. Lovat, D. Pantarotto, L. Lagostena, B. Cacciari, M. Grandolfo, M. Righi, G. Spalluto, M. Prato, L. Ballerini, *Nano Lett.* **2005**, *5*, 1107.
[25] N. W. S. Kam, E. Jan, N. A. Kotov, *Nano Lett.* **2009**, *9*, 273.
[26] S. Y. Park, J. Park, S. H. Sim, M. G. Sung, K. S. Kim, B. H. Hong, S. Hong, *Adv. Mater.* **2011**, *23*, H263.
[27] G. Jenkins, K. Kawamura, *Polymeric Carbon – Carbon Fibre, Glass and Char*, Cambridge University Press, Cambridge, UK **1976**, 178.
[28] O. J. A. Schueller, S. T. Brittain, G. M. Whitesides, *Adv. Mater.* **1997**, *9*, 477.
[29] C. Wang, M. Madou, *Biosens. Bioelectron.* **2005**, *20*, 2181.
[30] M. F. L. De Volder, R. Vansweevelt, P. Wagner, D. Reynaerts, C. Van Hoof, A. J. Hart, *ACS Nano* **2011**, *5*, 6593.
[31] R. Du, S. Ssenyange, M. Aktary, M. T. McDermott, *Small* **2009**, *5*, 1162.
[32] H. Xu, K. Malladi, C. Wang, L. Kulinsky, M. Song, M. Madou, *Biosens. Bioelectron.* **2008**, *23*, 1637.
[33] J. Mitra, S. Jain, A. Sharma, B. Basu, *Carbon* **2013**, *65*, 140.
[34] H. Kosonen, S. Valkama, a. Nykänen, M. Toivanen, G. ten Brinke, J. Ruokolainen, O. Ikkala, *Adv. Mater.* **2006**, *18*, 201.
[35] B. Y. Park, L. Taherabadi, C. Wang, J. Zoval, M. J. Madou, *J. Electrochem. Soc.* **2005**, *152*, J136.
[36] P. C. Georges, P. A. Janmey, *J. Appl. Physiol.* **2005**, *98*, 1547.
[37] M. N. Helmus, D. F. Gibbons, D. Cebon, *Toxicol. Pathol.* **2008**, *36*, 70.
[38] L. Amato, S. S. Keller, A. Heiskanen, M. Dimaki, J. Emnéus, A. Boisen, M. Tenje, *Microelectron. Eng.* **2012**, *98*, 483.
[39] N. M. Alves, I. Pashkuleva, R. L. Reis, J. F. Mano, *Small* **2010**, *6*, 2208.
[40] S. J. Lee, G. Khang, Y. M. Lee, H. B. Lee, *J. Colloid Interface Sci.* **2003**, *259*, 228.
[41] A. J. Downard, *Electroanalysis* **2000**, *12*, 1085.
[42] M. Hirabayashi, B. Mehta, N. W. Vahidi, A. Khosla, S. Kassegne, *J. Micromech. Microeng.* **2013**, *23*, 1.

[43] M. T. Khorasani, H. Mirzadeh, S. Irani, *Radiat. Phys. Chem.* **2008**, *77*, 280.
[44] Y. Y. Yan, N. Gao, W. Barthlott, *Adv. Colloid Interface Sci.* **2011**, *169*, 80.
[45] Y. Gao, X. Chen, S. Gupta, K. D. Gillis, S. Gangopadhyay, *Biomed. Microdevices* **2008**, *10*, 623.
[46] A. N. Patel, S. Tan, T. S. Miller, J. V Macpherson, P. R. Unwin, *Anal. Chem.* **2013**, *85*, 11755.
[47] M. Fryda, T. Matthée, S. Mulcahy, A. Hampel, L. Schafer, I. Troster, *Diam. Relat. Mater.* **2003**, *12*, 1950.
[48] S. H. Duvall, R. L. Mccreery, *J. Am. Chem. Soc.* **2000**, *122*, 6759.
[49] A. B. Kaufman, *Appl. Phys. Lett.* **1972**, *21*, 231.
[50] H. O. Pierson, *Handbook of Carbon, Graphite, Diamond and Fullerenes* Noyes Publications, Park Ridge, USA **1993** 43–69.
[51] S. Ranganathan, R. McCreery, S. M. Majji, M. Madou, *J. Electrochem. Soc.* **2000**, *147*, 277.
[52] A. Singh, J. Jayaram, M. Madou, S. Akbar, *J. Electrochem. Soc.* **2002**, *149*, E78.
[53] A. Dalmia, C. C. Liu, R. F. Savinell, *J. Electroanal. Chem.* **1997**, *430*, 205.
[54] C. Amatore, S. Arbault, M. Guille, F. Lemaître, *Chem. Rev.* **2008**, *108*, 2585.
[55] L. A. Greene, G. Rein, *Brain Res.* **1977**, *129*, 247.
[56] E. G. Seiz, M. Ramos-Gómez, E. T. Courtois, J. Tønnesen, M. Kokaia, I. Liste Noya, A. Martínez-Serrano, *Exp. Cell Res.* **2012**, *318*, 2446.
[57] F. Lemaître, M. G. Collignon, C. Amatore, *Electrochim. Acta* **2014**.